

RECENT RESEARCH PROGRAMS OF THE MuPAL-ε RESEARCH HELICOPTER

Yoshinori OKUNO, Naoki MATAYOSHI, and Hirokazu ISHII

Helicopter Team, Flight Test Technology Center

Institute of Space Technology and Aeronautics, Japan Aerospace Exploration Agency

Keywords: Helicopter, Flight Test, Atmospheric Turbulence, Acoustic Noise, GPS

Abstract

This paper summarizes recent research programs being carried out by the Japan Aerospace Exploration Agency (JAXA) using its research helicopter MuPAL-ε. Emphasis is on two major research fields; the measurement and evaluation of atmospheric turbulence, and research on noise abatement flight. Other topics such as GPS based navigation systems are also introduced.

1 Introduction of MuPAL-ε

JAXA has been operating its MuPAL-ε research helicopter (Figs. 1.1 and 1.2, [1]), based on a

Mitsubishi Heavy Industries MH2000A, Japan's first domestically developed commercial helicopter, since April 2000. MuPAL-ε is designed to support research in the fields of helicopter guidance, navigation, and control, especially pilot-vehicle interfaces, and is equipped with four systems for flight experiments: a data acquisition system that provides extensive flight data; a cockpit display system driven by a high-performance graphics computer that enables researchers to experiment with various types of display; a video image recording system that captures external views to allow image processing technology to be applied to helicopter navigation; and a variable stability flight control system that realizes different dynamic responses to pilot control inputs. Installed sensors include a hybrid DGPS/INS (Differential Global Positioning System/Inertial Navigation System) that produces highly accurate navigation data using a medium-wave radio signal broadcast by the Japan Coast Guard DGPS stations, which provide complete coverage for the coastal areas of Japan. This paper summarizes recent research activities and some future plans utilizing MuPAL-ε research helicopter.



Fig. 1.1 Research helicopter MuPAL-ε (MH2000A) and research airplane MuPAL-α (Do228).

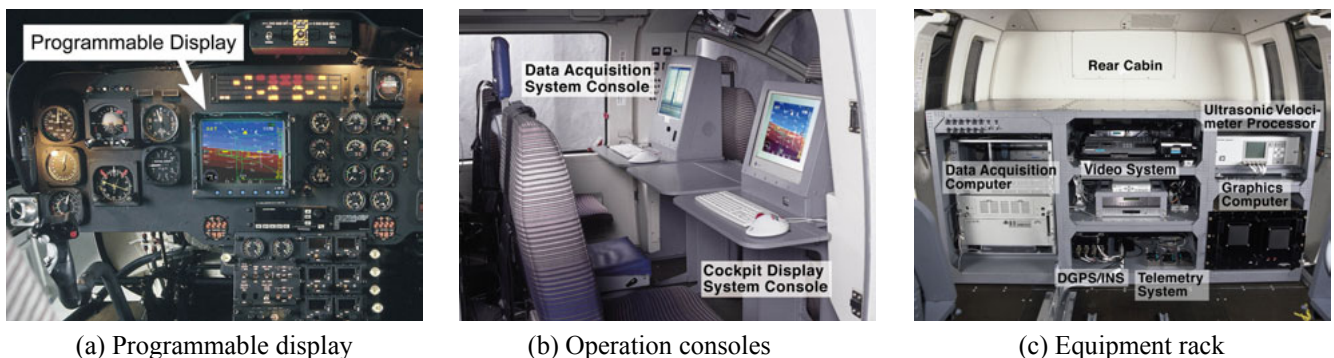


Fig. 1.2 MuPAL-ε experimental system layout.

2 Evaluation of Atmospheric Turbulence

2.1 Development of Ultrasonic Velocimeter

JAXA has been studying the use of aircraft to measure atmospheric turbulence. MuPAL-ε is equipped with an original air data sensor called an ultrasonic velocimeter (USV, Fig. 2.1.1), which can measure 3-axis airspeeds at a high sampling rate (20 Hz) even in low-speed flight, where a Pitot-static system is ineffective. Highly accurate turbulence data are obtained using airspeed data from the USV and ground speed data from the DGPS/INS. Extensive flight tests have been conducted to determine the position error at the USV sensor location, i.e., the effects of the flow around the fuselage and rotor wake. The expected overall wind speed accuracy and spatial resolution are 2 kt and 1 m respectively at a flight speed of 40 kt.



Fig. 2.1.1 Ultrasonic velocimeter installation.

2.2 Evaluation of Severe Local Turbulence

MuPAL-ε's wind measurement system was used for the qualification of a planned cliff-top heliport, located on Aogashima Island (Fig. 2.2.1, [2]). The part of the island where the heliport is to be constructed is surrounded by steep cliffs that may cause severe local turbulence. MuPAL-ε acquired wind data flying around and over the planned heliport site, and performed takeoffs and landings to evaluate the effects of local turbulence on flight safety.

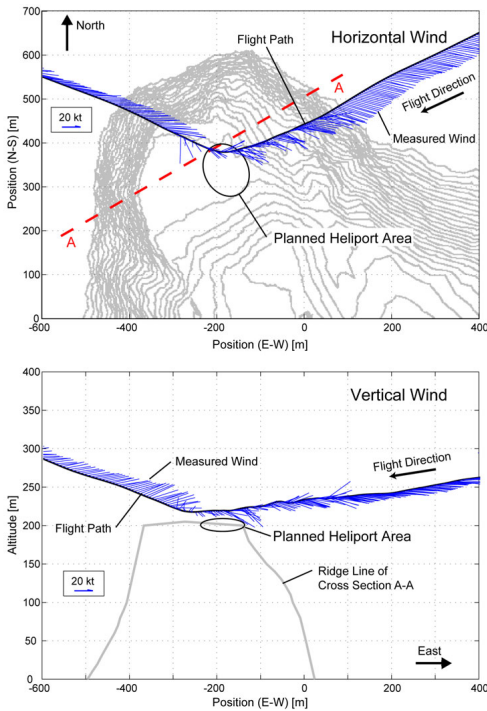
Figure 2.2.2 (a) and (b) show examples of measured turbulence data and helicopter response in winds of approximately 40 kt (a nearly 10% possible condition throughout the year in this area). In these cases, turbulence over

the planned heliport was so strong that the pilot abandoned hovering. Although the pilot tried to maintain airspeed at 70-80 kt during approach, airspeed fell abruptly to under 20 kt when flying over the planned heliport because the 40 kt head wind suddenly disappeared there. Vertical wind variation of over 20 kt (\cong 2000 fpm) was also observed, and the pilot was forced to use excessive engine power control as shown in Fig. 2.2.2 (b). The variation of vertical acceleration was also large, with a peak-to-peak range of almost 1 G. Considering these flight test results, wind limitations will be imposed at this heliport to ensure the safety of operations.

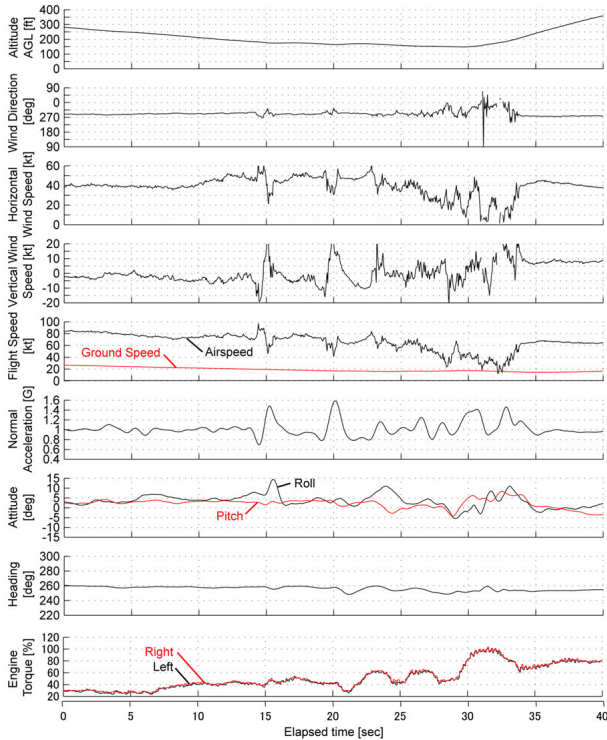
The Japan Weather Association performed CFD (computational fluid dynamics) analysis to clarify the turbulence around the planned heliport. Figure 2.2.3 compares the measured wind speed variations during level flight at a height of nearly 30 m above the planned heliport surface and the turbulent kinetic energy calculated by CFD analysis. Although CFD analysis is useful to survey the effects of various uniform wind speeds and directions, some discrepancies are observed between the calculated and measured local turbulence distributions; CFD analysis indicates that the strongest turbulence is generated at the windward cliff edge, while the measured turbulence was severest at the middle of the cliff top surface. This may be due to the turbulence model used in the CFD analysis (a $k-\epsilon$ model), and another CFD program based on an LES (large eddy simulation) turbulence model is currently being developed by the Tokyo Institute of Technology.



Fig. 2.2.1 Overview of Aogashima Island.



(a) Measured wind components along the flight path



(b) Helicopter response

Fig. 2.2.2 Flight measurement of severe local turbulence around cliff edges at Aogashima Island.

On the basis of the flight test data and CFD results, a wind turbulence model for a flight simulator (Fig. 2.2.4) is being developed to

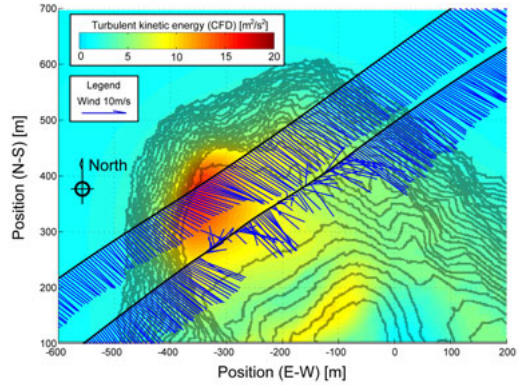


Fig. 2.2.3 Comparison of measured and calculated turbulence distributions.



Fig. 2.2.4 Flight simulator setup.



Fig. 2.2.5 Display image of 3D turbulence information.

evaluate the wind limitations at this heliport. Development of a cockpit turbulence display (Fig. 2.2.5) using this simulator is also on going.

2.3 Response to Wake Turbulence

In order to realize helicopter operations at large and congested airports, a study is being carried out of the effects of large airplane wake vortices on helicopter flight safety. While many research programs, such as AVOSS in the USA or WakeNet 2 in Europe, focus on the effects of wake turbulence on fixed-wing aircraft, less efforts have been made for helicopters.

Figure 2.3.1 shows the results of piloted flight simulation tests when the vortex wake of a large airplane (Boeing 747) is encountered by a helicopter (MH2000A) and an airplane (Dornier Do228, Fig. 1.1). Although these two aircraft are of similar size and weight, the response of the helicopter is much milder than that of the airplane, which implies that the separation between a helicopter and a preceding airplane can be smaller than that for a fixed-wing airplane.

A lidar (laser radar) system has been installed at Sendai airport by the Electronic Navigation Research Institute (ENRI) to measure wind speeds in the vortex wake field. It is planned to use these data to improve the accuracy of the flight simulator wake turbulence model.

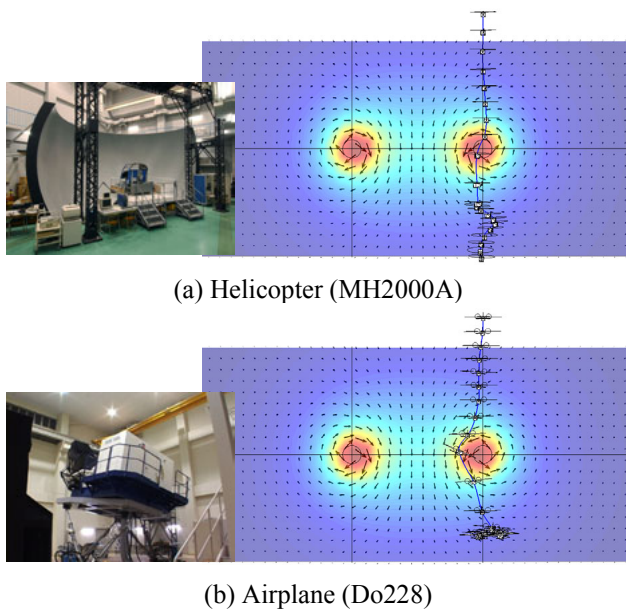


Fig.2.3.1 Piloted flight simulation test results of response to a large airplane's vortex wake.

2.4 Future Plan - Development of Lidar

JAXA has been studying Doppler lidar as an airborne remote sensor for wind turbulence [3]. The current system, developed by Mitsubishi Electric Corporation, uses $1.5 \mu\text{m}$ coherent pulsed laser light and features all-fiber components, enabling small size and weight, high reliability, and great flexibility of installation. Flight test evaluation of this system has been conducted using JAXA's Beechcraft 65 research airplane (Fig. 2.4.1). The final goal of this



Fig. 2.4.1 Lidar installation on B65 research airplane.

program is to achieve a clear air turbulence (CAT) detection performance of 5 nm at the cruising airspeed and altitude of large commercial airplanes, e.g., Mach 0.85 at 30,000 ft.

The lidar turbulence detection system is also expected to be useful for helicopters, especially when operating in mountainous areas or from roof-top helipads on high-rise buildings. For this purpose, the detecting range can be much shorter, e.g., 1 nm, but higher spatial and temporal resolutions are required. Flight evaluation by MuPAL- ϵ of a preliminary lidar system is currently scheduled.

3 Noise Abatement Flight

This section introduces acoustic flight experiments using various measurement methods. The data obtained contribute to understanding the mechanism of noise generation and to the development of a helicopter noise model. The end goal is to establish helicopter noise abatement operations.

3.1 Measurement from Ground

Since the noise generated by a helicopter has different directivities in the directions of the main rotor tip-path plane and normal to it, flight experiments were conducted in which MuPAL- ϵ flew banked turns and the noise on the ground was recorded by microphones located in the 'in-

plane' and normal directions (Fig. 3.1.1, [4]). A 'Tunnel In the Sky' display (see 4.2) provided guidance to the pilot to precisely control flight path and bank angle.

Figure 3.1.2 shows the results of these experiments in comparison with similar test results using JAXA's MuPAL-α fixed-wing research airplane (Dornier Do228, Fig. 1.1). It can be seen in Fig. 3.1.2 (a) that the A-weighted OASPL (overall sound pressure level) of the helicopter is loudest in forward direction, 30 degrees below the main rotor tip-path plane. The lateral noise directivity pattern of the airplane, shown in Fig. 3.1.2 (b), is more complicated, caused by interaction between the noise from its two propellers and the airframe, such as reflection and refraction.

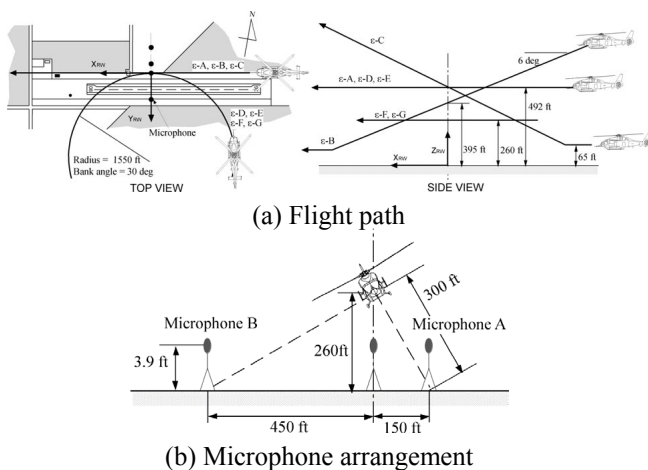


Fig. 3.1.1 Acoustic flight test setup.

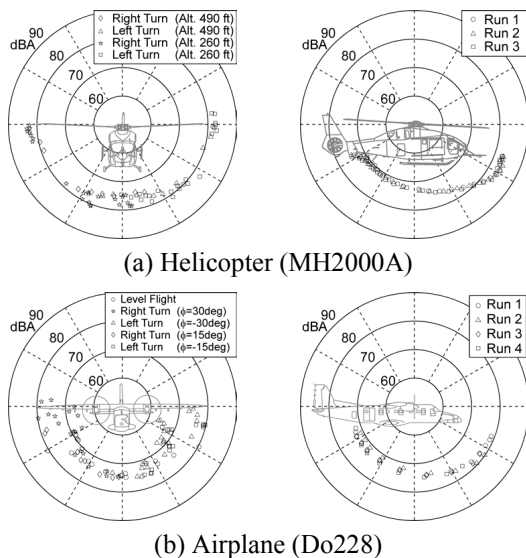


Fig. 3.1.2 Noise directivity pattern measured by ground microphones.

3.2 Microphone Array

Measurements using microphone array systems (Fig. 3.2.1) developed by JAXA's Aeronautical Environment Technology Center have made to determine the precise distribution of noise from each source, e.g., main and tail rotor aerodynamic noise, engine noise, and gearbox mechanical noise. Fig. 3.2.2 shows the results of a ground rotor run test using the 'handy' type system (13 microphones are arranged in a 33cm x 33cm hand-held unit) shown in Fig. 3.2.1 (a). Noise at 1,600 Hz, which is the third harmonic of the tail rotor blade passing frequency of 525 Hz, emanates from the tail rotor as shown in Fig. 3.2.2 (a). Figs. 3.2.2 (b, c), which show the distributions of noise frequencies of 6,900 Hz and 8,000 Hz, respectively clarify the gearbox noise and the compressor blade passing noise. Flight experiments using a ground based microphone array system (28 microphones in 10m x 10m area) shown in Fig. 3.2.1 (b) have also been conducted, and analysis of the measured data is currently in progress.

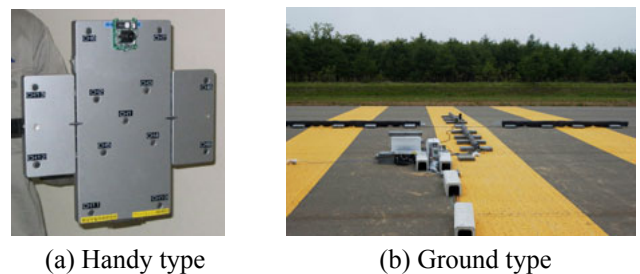


Fig. 3.2.1 Microphone array.

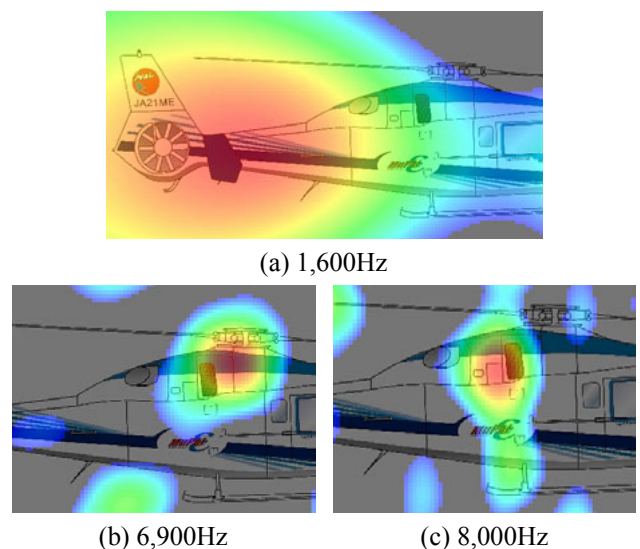


Fig. 3.2.2 Noise distributions at various frequencies.

3.3 Measurement by Onboard Microphone

In order to obtain precise noise waveforms emitted from a helicopter, a microphone is installed at the tip of MuPAL-ε's nose boom as shown in Fig. 3.3.1. This microphone installation greatly reduces or eliminates the influences of attenuation of noise during propagation and the Doppler effect, which are unavoidable in ground measurement.

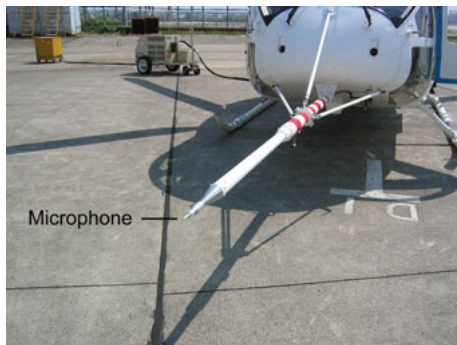


Fig. 3.3.1 Onboard microphone installation.

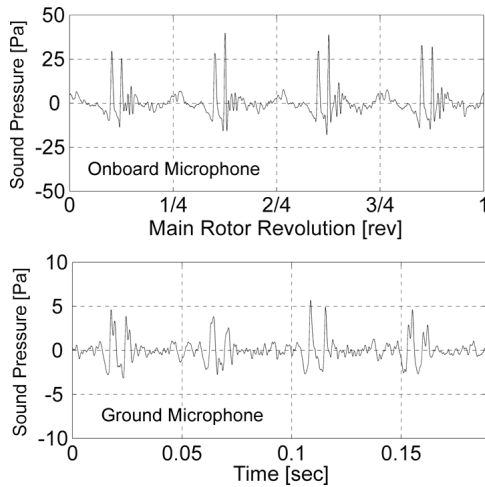


Fig. 3.3.2 BVI noise measured by onboard and ground microphones.

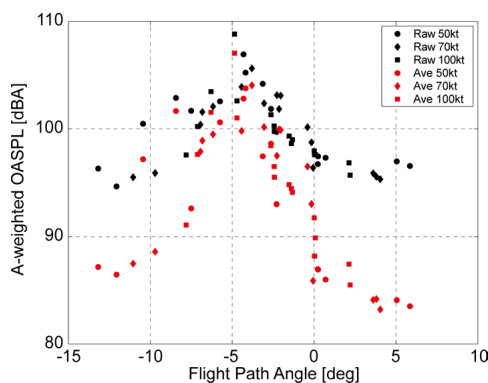


Fig. 3.3.3 Noise measured by onboard microphone.

MuPAL-ε was flown in a 600 fpm descent at an airspeed of 70 kt to measure Blade-Vortex Interaction (BVI) noise. The results, shown in Fig. 3.3.2, demonstrate the effectiveness of the onboard microphone by its ability to obtain a sharper BVI noise waveform than ground microphone.

A main rotor 1/rev signal was used to synchronize the measured data to the main rotor revolutions for averaging. The red symbols in Fig. 3.3.3 shows the results in which the sound pressures of 32 consecutive main rotor revolutions were averaged to eliminate noise from sources other than the main rotor, while the black symbols include noise from all sources. Main rotor noise becomes dominant at a descent angle of about 5 degrees, where BVI noise tends to occur.

3.4 Future Plans - Noise Abatement Flight

Development of a noise model that will enable the precise estimation of helicopter noise in the area under the flight path is currently on going. The influences of the vertical wind profile, temperature, and humidity must be taken into account. This model is being used to develop a cockpit display (Fig. 3.4.1) which shows the predicted noise footprint to pilots in real time and assists them in minimizing noise impact to neighborhoods. Calculation of the optimal flight path which minimizes noise impact on the ground taking into account land use information, e.g., schools, hospitals, residential areas, rivers, forests, etc., is also being carried out in collaboration with the University of Tokyo. The resulting optimal path will be demonstrated in actual flight tests by applying ‘Tunnel In the Sky’ display (see 4.2).

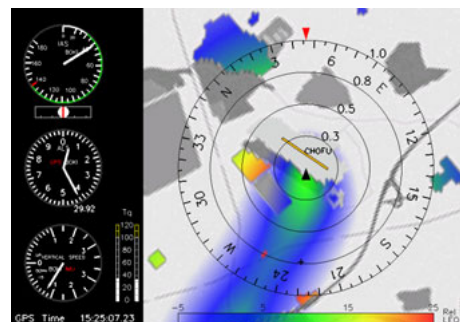


Fig. 3.4.1 Display image of onboard noise estimation.

4 GPS Navigation

4.1 GPS Installation Problems

MuPAL-ε’s GPS antenna is installed on the right-hand side of the fuselage above the cockpit. The rotor and engine structures located above the antenna cause GPS signal masking and multi-path error. Since the elevation angle from the GPS antenna surface to the top of the main rotor head is about 15°, there is no significant masking of antenna coverage by the rotor head when the helicopter is flying straight. However, the probability of the rotor head masking the GPS signal increases when the helicopter banks to the right.

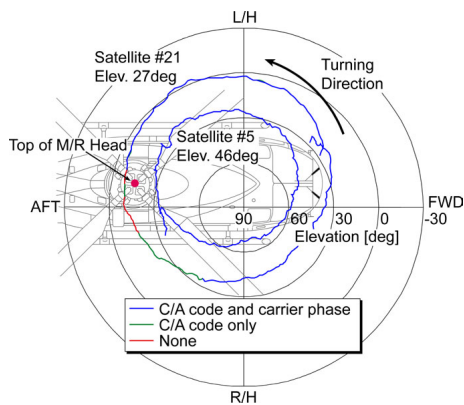


Fig. 4.1.1 Flight data of GPS signal masking by helicopter rotor and engine structures.

Figure 4.1.1 exemplifies flight test results of the statuses of received GPS signals, shown as a function of elevation and azimuth angle from the GPS antenna surface to the satellites, during a 360° right turn at a fixed bank angle of 15°. The blue lines indicate the area where both C/A (coarse and acquisition) code and carrier phase signals could be obtained; the green lines indicate the area where only the C/A code signal could be obtained; and the red lines indicate the area where neither signal could be obtained. It can be seen that neither signal from satellite #21 (at an elevation of 27° above the horizon) could be received when it was behind the main rotor head. While the C/A code signal recovers soon after the satellite comes into sight of the antenna again, recovery of the carrier phase signal takes much longer (nearly 10 sec in this case). When the satellite is sufficiently high above the horizon (e.g., 46° for satellite #5), both signals can be received stably without being masked by the rotor head. Since the KGPS (kinematic GPS) process requires continuous carrier phase signals from at least four satellites, it is difficult to apply this technique when the helicopter is maneuvering.

Figure 4.1.2 shows the effects of multi-path error observed during banked turning flight.

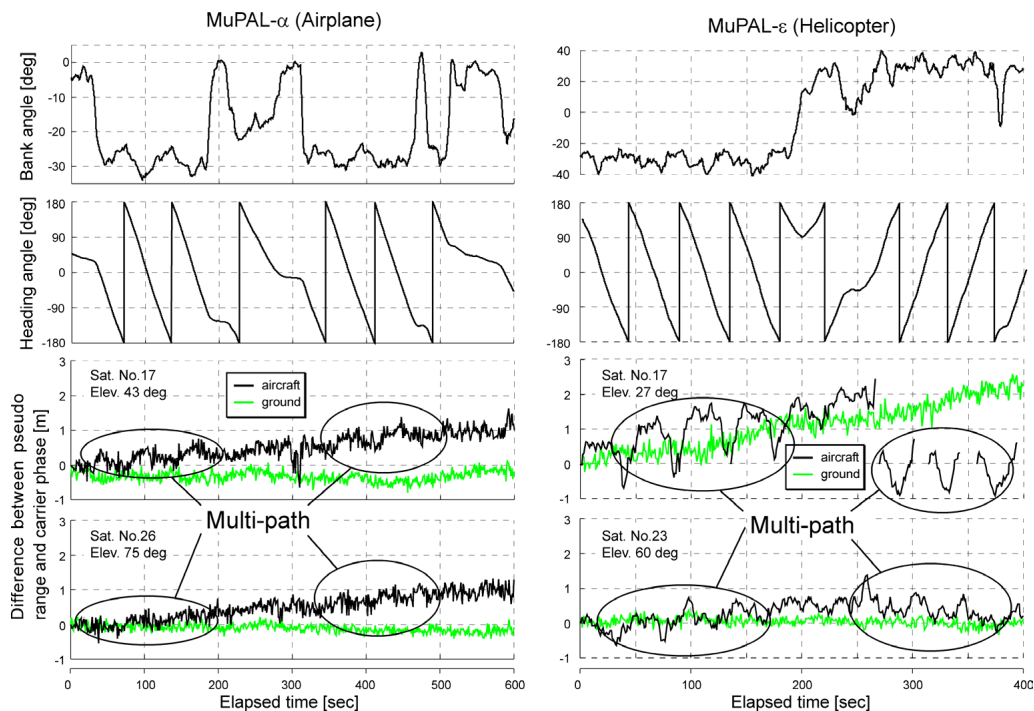


Fig. 4.1.2 Multi-path error due to aircraft structures.

The results for the fixed-wing MuPAL- α are also shown for comparison. MuPAL- α 's GPS antenna is installed on the top of the center fuselage section, with no significant obstructions around the antenna. The two upper graphs show aircraft bank and heading angles respectively recorded during left and right turning flight, and the two lower graphs show the difference between the pseudo-range and carrier phase signals received by onboard and ground-based receivers for two GPS satellites. In both the MuPAL- α and MuPAL- ε results, periodic variations that correlate with aircraft heading angle can be seen only in the onboard receiver signals. These variations are caused by multi-path error, and their amplitudes become large for low elevation satellites. Note that the variation amplitudes are quite different between MuPAL- α and MuPAL- ε ; MuPAL- ε 's variation is approximately ± 1 m, greater than that of MuPAL- α . MuPAL- ε 's main rotor and engine structures located above the GPS antenna cause these strong multi-path effects.

4.2 Research on 3D/4D Guidance System

JAXA and ENRI have been carrying out a research program called New Operational Concept using Three-dimensional Adaptable Route Navigation (NOCTARN), aimed at developing an aircraft operations concept that can reduce the impact of noise on communities while enhancing the capacity and operational efficiency of airports, focusing on regional airports and small aircraft and helicopters, by using precisely-defined trajectories which are shared between aircraft and ground. Since the proposed operational concept requires pilots to fly along curved trajectories while communicating with the controller, and differs from both conventional Visual Flight Rules (VFR) and Instrumental Flight Rules (IFR) procedures, considerable attention has been paid to the system design and evaluation of the pilot human machine interface and procedures. Extensive flight tests and flight simulations have been conducted to evaluate the feasibility of these procedures and the pilot interface. Figure 4.2.1 shows an example of proposed



Fig. 4.2.1 Display image of 4D guidance system.

pilot display which includes a 'Tunnel In the Sky' guidance display, a Controller-Pilot Data Link Communication (CPDLC) message menu, and a Cockpit Display of Traffic Information (CDTI) [5]. The positions and also the current trajectories of other aircraft in the vicinity are obtained via an ADS-B (Automatic Dependent Surveillance – Broadcast) like data link system and are presented on the CDTI.

4.3 GPS Pseudolite Flight Experiment

JAXA has proposed a new positioning and navigation service using GPS pseudolites (PL) installed on the High Altitude Platforms System (HAPS) [6]. If pseudolites were mounted on HAPS platforms, their GPS-like signals would be stable augmentation that would improve the performance of GPS positioning. In order to establish the necessary basic technologies, augmentation tests were conducted using a pseudolite installed on MuPAL- ε (Fig. 4.3.1). The position of the pseudolite antenna on the bottom of the fuselage, which is analogous to the GPS 'precise ephemeris', was precisely determined by the inverted GPS method. The results also demonstrate the efficacy of integrating the pseudolite signal with GPS.

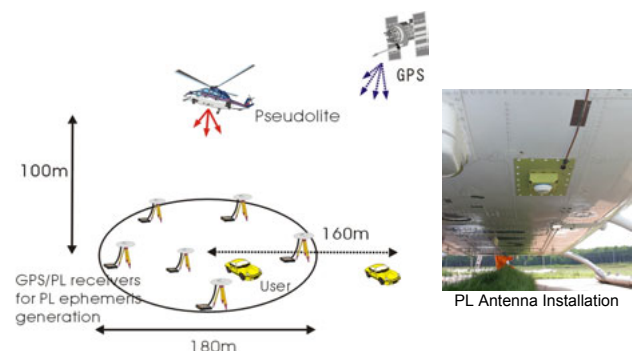


Fig. 4.3.1. GPS/PL flight test setup.

4.4 GPS/IFR Route Preliminary Investigation

Helicopters IFR operations are not common in Japan. One reason for this is that the minimum en-route altitude of existing IFR routes is too high for helicopters. Japan has many mountains of 3,000–10,000 ft throughout which block NAV/COM radio wave signals. The MTSAT Satellite-based Augmentation System (MSAS), scheduled to begin operating in 2005, will provide an alternative navigation system with coverage independent of the location of ground stations; however, communication must still depend on ground-based systems for the present.

MuPAL-ε is being used for the preliminary investigation of low altitude IFR routes suitable for helicopters proposed by the ‘Research Committee on Helicopter Flight Safety and IFR Operations’ (Fig. 4.4.1).

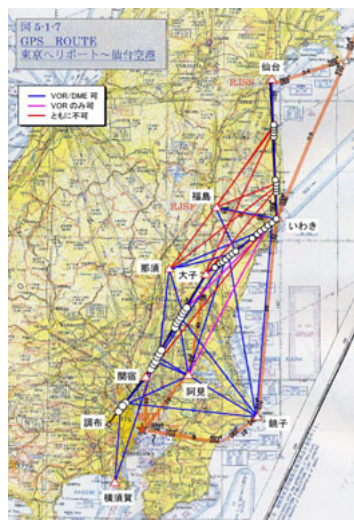


Fig. 4.4.1 Flight investigation of NAV/COM radio signal statuses.

5 Other Research

5.1 Mega-Float ILS Evaluation

The Instrument Landing System (ILS) is prone to signal errors due to such factors as ground surface characteristics and obstacles near the transmitting antennas. A flight test method was proposed to evaluate such radio anomalies that exploits the particular capabilities of helicopters, such as hover, vertical climb and sideways flight, to map the ILS signal distribution around the approach path (Fig. 5.1.1).

This flight test method, named ‘ILS sweep’, was used to evaluate an ILS situated on the Mega-Float (Fig. 5.1.2), a large floating marine structure with a 1,000m x 60m runway, as its unique steel structure was expected to cause radio anomalies [7]. Some characteristic ILS signal errors were observed in the flight tests,

which corresponded well with numerical analyses conducted by ENRI as shown in Fig. 5.1.3. Large sinusoidal variation of the glide slope error (ΔGS , indicated as A) is due to the influence of radio waves diffracted by the edges of the Mega-Float structure. A small arch-shaped variation of ΔGS (indicated as B) is also seen at just below the nominal glide path, and this is due to the influence of a ‘dolphin’ structure located beside the runway. At low altitudes ($GS > 2$ dots), ΔGS becomes large due to basic GS characteristics (indicated as C). The proposed ILS evaluation method was thus demonstrated to be effective for directly measuring the spatial distribution of ILS signal errors and clarifying their causes.

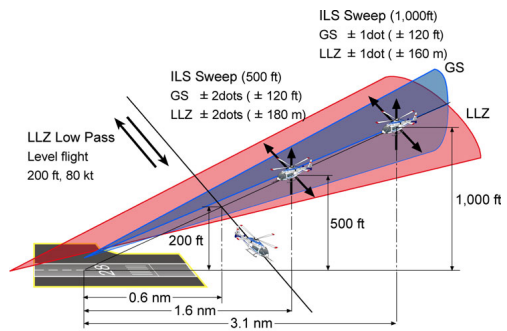


Fig. 5.1.1 ‘ILS sweep’ flight test patterns.



Fig. 5.1.2 Mega-Float experimental airport.

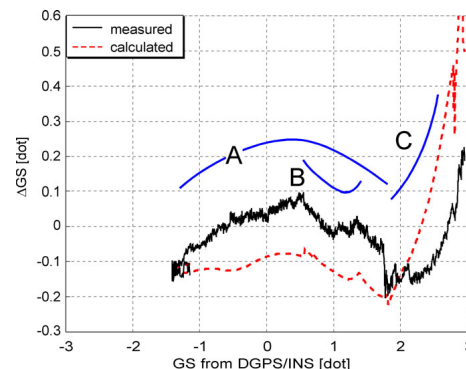


Fig. 5.1.3 Comparison of measured and analytical glide slope (GS) signal errors.

5.2 Flight Characteristics Evaluation

In order to evaluate the fidelity of JAXA's helicopter flight simulator, especially at low altitudes, a pirouette maneuver defined in the ADS-33 rotorcraft handling qualities requirements, was introduced as it is considered as an excellent multi-axis task near the ground.

Figure 5.2.1 shows a test area prepared at the Taiki airfield in northern Japan and a flight simulator visual scene. Although the flight simulator has a motion base cockpit system, it was not used because the motion drive algorithm is not completely tuned to precisely synchronize with the visual system. Figure 5.2.2 shows a comparison of the flight test and simulation test results. The goal of this research is to improve the simulator's flight dynamics model, motion algorithm, and visual scene to achieve a comparable level of task performance as in actual flight.



Fig. 5.2.1 Pirouette flight test area and simulator setup.

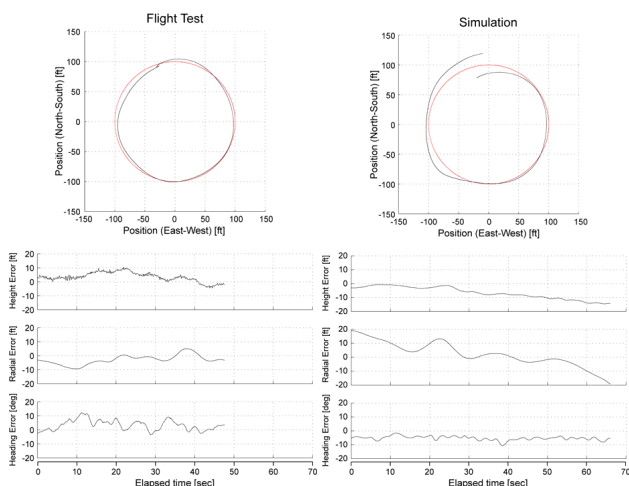


Fig. 5.2.2 Comparison of flight and simulation test results of pirouette task performance.

5.3 Development of Lunar Landing Radar

JAXA's Institute of Space and Astronautical Science is developing a landing radar (radio

altimeter/velocimeter) as an essential navigation sensor for lunar or planetary landing. This C band (4.3 GHz) radar has one wide vertical beam for radio altimetry and three tilted beams to measure velocity. The required maximum range is 3.5 km altitude, and Barker code pulse compression is used at long ranges. MuPAL- ϵ is used as a test bed for this system to obtain field test data (Fig. 5.3.1).

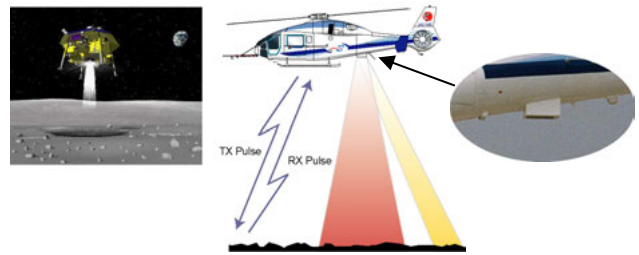


Fig. 5.3.1 Field test of lunar landing radar.

6 Concluding Remarks

MuPAL- ϵ is being well-utilized as an experimental tool in a diverse range of research areas. We hope it will contribute to the development of safer helicopter operations.

References

- [1] Okuno, Y, et al. Development of a new research helicopter MuPAL- ϵ . *American Helicopter Society 57th Annual Forum*, Washington, DC, 9-11 May 2001.
- [2] Matayoshi, N, et al. Measurement and evaluation of cliff-top turbulence using a research helicopter, *30th European Rotorcraft Forum*, Marseilles, France, 14-16 Sep 2004.
- [3] Asaka, K, et al. A 1.5 μm all-fiber pulsed airborne Doppler lidar system. *International sessions in 41st Aircraft Symposium*, Nagano, Japan, 8-10 Oct 2003.
- [4] Ishii, H, et al. Flight experiments for aircraft noise measurement using 'Tunnel In the Sky' display. *AIAA Atmospheric Flight Mechanics Conference*, Monterey CA, 5-8 Aug 2002, AIAA Paper 2002-4880.
- [5] Nojima, T, et al. Flight demonstration of a new operational concept using TDMA data link system. *24th ICAS*, Yokohama, Japan, 29 Aug-3 Sep 2004.
- [6] Tsujii, T, et al. Preliminary tests of GPS/HAPS positioning system using a pseudolite on helicopter. *16th IFAC Symposium on Automatic Control in Aerospace*, St. Petersburg, Russia, 14-18 June 2004.
- [7] Matayoshi, N, et al. Evaluation of ILS radio anomalies by helicopter flight test and numerical analysis. *Journal of the American Helicopter Society*, Vol. 47, No. 3, 2002.